Journal of Anatomy

J. Anat. (2016) **228**, pp190–202 doi: 10.1111/joa.12383

Methods and theory in bone modeling drift: comparing spatial analyses of primary bone distributions in the human humerus

Corey M. Maggiano,[1,2] Isabel S. Maggiano,[1,3] Vera G. Tiesler,[4] Julio R. Chi-Keb[4] and Sam D. Stout[5]

[1]*Department of Anthropology, University of West Georgia, Carrollton, GA, USA*
[2]*Department of Anthropology, University of Western Ontario, London, ON, Canada*
[3]*Department of Anatomy and Cell Biology, University of Saskatchewan, Saskatoon, SK, Canada*
[4]*Department for Anthropological Sciences, Universidad Autónoma de Yucatán, Mérida, Yucatán, Mexico*
[5]*Department of Anthropology, The Ohio State University, Columbus, OH, USA*

Abstract

This study compares two novel methods quantifying bone shaft tissue distributions, and relates observations on human humeral growth patterns for applications in anthropological and anatomical research. Microstructural variation in compact bone occurs due to developmental and mechanically adaptive circumstances that are 'recorded' by forming bone and are important for interpretations of growth, health, physical activity, adaptation, and identity in the past and present. Those interpretations hinge on a detailed understanding of the modeling process by which bones achieve their diametric shape, diaphyseal curvature, and general position relative to other elements. Bone modeling is a complex aspect of growth, potentially causing the shaft to drift transversely through formation and resorption on opposing cortices. Unfortunately, the specifics of modeling drift are largely unknown for most skeletal elements. Moreover, bone modeling has seen little quantitative methodological development compared with secondary bone processes, such as intracortical remodeling. The techniques proposed here, starburst point-count and 45° cross-polarization hand-drawn histomorphometry, permit the statistical and populational analysis of human primary tissue distributions and provide similar results despite being suitable for different applications. This analysis of a pooled archaeological and modern skeletal sample confirms the importance of extreme asymmetry in bone modeling as a major determinant of microstructural variation in diaphyses. Specifically, humeral drift is posteromedial in the human humerus, accompanied by a significant rotational trend. In general, results encourage the usage of endocortical primary bone distributions as an indicator and summary of bone modeling drift, enabling quantitative analysis by direction and proportion in other elements and populations.

Key words: anthropology; bioarchaeology; bone; growth; histology; histomorphometry; method; modeling; primary bone.

Introduction

Understanding structure and its connection to function is central to all inquiries targeting or involving bone. This includes both deductive and inductive applications of skeletal biology, whether the intention is to construct experiments testing theory in medical science, or to reconstruct experience using theory in archaeological or forensic science. In these endeavors, we rely on a detailed understanding of bone growth and mechanical adaptation accounting for morphological change. We also rely on accurate methods for comparing variation between individuals, subpopulations, or populations. However, significant aspects of skeletal biology remain obscured, despite their importance in this regard. This is due in part to understandable limitations in experimental design regarding human subjects (or tissues), and to the unique material properties of hard tissues, challenging our attempts at observation. Relatively little is known about how a given human bone achieves its existing diametric morphology, total cortical area, shape, and orientation with respect to other elements or how disease may affect these processes. We know that bone tissue 'records' some of this ontogenetic, adaptive,

Correspondence
Corey M. Maggiano, Department of Anthropology, University of West Georgia, 1601 Maple St., Carrollton, GA 30118, USA.
E: coreymaggiano@gmail.com

Accepted for publication *20 August 2015*
Article published online *15 October 2015*

and disease process information in the character and distribution of different tissues within cortical bone. This is due to bone's biostratigraphic nature, preserving its formative (and even some resorptive) history within its own microstructure (Enlow, 1962; Garn, 1970, 1972; Goldman et al. 2009; Maggiano et al. 2011; Maggiano, 2012b). The largest part of this history is written by the activity of a bone's inner and outer membranes (envelopes) through the process of intramembranous ossification (Martin et al. 1998). Understanding the microstructural remnants of this process is important for anatomical, clinical, and bioarchaeological or forensic interpretations.

Unfortunately, quantitative means of comparison for periosteal and endosteal primary bone growth and adaptation has lagged behind techniques targeting secondary tissues formed during intracortical bone turnover and repair. The result is that variance in human primary bone growth and adaptation, major vectors of growth per modular biomechanical region, or even for entire elements, is unknown in most cases. Developmental changes in human diaphyseal morphology and its variation in healthy and diseased contexts are even more poorly understood. It has been difficult to even visualize primary bone deposits as events, or 'phases' of formation, which are macroscopic in scale but are identified using microscopic and typically qualitative indicators (Maggiano et al. 2011; Maggiano, 2012b). Another limitation is the lack of methods suitable for the statistical comparison of primary bone distributions and the lack of integration between microscopic (histomorphological) and cross-sectional geometric perspectives on bone structure and process.

The current project proposes and compares two modified methods for the spatial and statistical analysis of primary and secondary microscopic bone distributions in long bone diaphyses. The first uses traditional point-count microscopy modified using a starburst sampling pattern permitting assessment of spatial distributions of counted cross-sectional features and the summary of biomechanically significant growth vectors. In the second method, areas and tissue type distribution summaries are generated using hand-drawn and digitally collected data using a novel 45° stitched microphotographic technique. Data collected through these two methods should be similar, but could exhibit different application dependent strengths and weaknesses.

Background

Long bones form from a mix of two main processes: (i) elongation through endochondral ossification and (ii) diametric growth via intramembranous bone formation at the periosteal and endosteal membranes (PEM). This diametric growth, called modeling, results in primary bone tissue, microstructurally presenting somewhere along a continuum between woven (rapidly deposited bone with disorganized collagen orientations) and lamellar bone (more slowly deposited bone laid down in thin sheets of lamellae with well-organized collagen). Other tissue types fall variously between these states, including fibrolamellar bone and true laminar bone (of which plexiform bone is one form), as reviewed elsewhere (De Ricqlès, 1976, 1991; Castanet et al. 2004; Bromage et al. 2009). Of importance here, however, is identifying how primary periosteal origin and endosteal origin tissues can be differentiated. For clarity, and following conventions outlined previously (Maggiano, 2012b), discrete or semi-discrete primary lamellar bone deposits are referred to here as 'formation phases' (Frost's 'packets' in 1973), and 'pericortex' (periosteal bone) or 'endocortex' (endosteal bone) are terms used to identify tissues formed by the respective membrane, rather than as arbitrary regions of the inner and outer cortex. The membranes themselves, the periosteum and endosteum, are quite different histologically and behaviorally (Hohmann et al. 1986; Martin et al. 1998) but produce extremely similar lamellar bone. Despite these similarities, the overall orientation and organization of lamellar bone differs between these two sources (see Maggiano, 2012b). The main and most striking difference is the presence of many longitudinal primary vessel canals in periosteal tissue, which are largely absent from endosteal tissue, lending the former a 'wavy' appearance and the latter a smooth or more 'dense' appearance. Also, since both are formed on opposite topography, one generally convex and the other concave, their bone formation phases are structured differently (Maggiano, 2012b). These differences aid in distinguishing the membrane of origin for primary tissues, even when considering smaller patches of primary bone located between other tissue types.

Because primary tissue has an immature vasculature and accrues microscopic damage from wear and tear, another process ensures sufficient vascular supply and the maintenance of the bone's material integrity through replacement of primary bone with secondary bone. This process is called remodeling (sometimes modified as 'intracortical remodeling') and is performed by bone's basic multicellular unit (BMU). The BMU removes old bone at its leading cutting cone, replacing it with newly deposited lamellar bone encasing an accompanying vessel system, forming a tubular, bull's-eye-like structure (~200 μm in diameter and often millimeters in length). The resulting bone structural unit (BSU) is called a secondary osteon, or Haversian system. Jee et al. (2007) provide a useful chart modified from Parfitt (1983) for comparing modeling and remodeling in scale and function (see also Maggiano, 2012b for information on differentiating modeling and remodeling microstructures).

Whereas remodeling requires prior resorption, bone modeling and growth do not. Resorption is still a vital part of the modeling process, however, and may immediately precede formation as part of morphological change. Often the textbook explanation of diaphyseal bone growth simplifies the periosteum as formative and the endosteum as resorptive. Although this is one way to effect net growth,

this simplification fails to include the distinctly asymmetric growth that can characterize the achievement of adult morphology. It has been well documented that bone tissue can form and resorb on opposite cortices in order to alter the curvature of the element or even its position relative to the rest of the skeleton. This process is called 'modeling drift' (Epker & Frost, 1965; Frost, 1973, 2001) or 'osseous drift' (Enlow, 1962), and is the focus of this study.

Bone growth, modeling, and modeling drift

Unfortunately, the difference between growth, bone modeling, and modeling drift has sometimes been left vague. These processes, although often simultaneous, are governed by different scales of hormonal and biomechanical input and accordingly affect different scales of bone morphological change. Each of them occurs at the PEM and so has been distinguished from intracortical or trabecular BMU activity.

Diametric bone growth simply deposits more tissue than is removed, whereas bone modeling accomplishes many different types of morphological change. The need for distinction is clear: not all bone modeling is growth and, likewise, not all bone modeling leads to drift. Growth could be envisioned as providing peak bone mass, whereas modeling sculpts the available tissue, fitting form to function. Bone modeling accomplishes vital aspects of development and adaptation, affecting curvature, cross-sectional geometry, position relative to articulations, metaphyseal reduction, and lamellar compaction (Maggiano, 2012b). These processes are most active during ages of skeletal growth, but continue to alter bone morphology into early maturity (as is suggested by the work of Garn, 1970, 1972, and Peck & Stout, 2008) and, to a lesser degree, even later in adulthood (Lazenby, 1990; Ruff et al. 2006). In fact, in the adult, it becomes particularly interesting that changes in adaptive morphology could transpire that do not yield increased size. The result of growth and modeling is a bone delicately balanced on the boundary between strength and mass, its morphology biomechanically adapted to the loading history of the element.

Sometimes, however, the modeling process is dominated by a modular or even whole element mechanical demand, resulting in a drifted cortex. Modeling drift deposits bone on one cortex while removing it on the opposite side (a process that must be mirrored by the endosteum to keep the medullary cavity centric with respect to the element's neutral axis). In effect, the long bone can grow transversely. Modeling drift achieves large-scale changes in diametric morphology that alter the bone's curvature or orientation with respect to other biomechanically important subcomponents of the element, the joint, or even the wider skeleton. Recently, there has been renewed interest in regional structural variation in cortical tissue within both anatomical (Goldman et al. 2005, 2009; McFarlin et al. 2008) and archaeological applications (Maggiano et al. 2011). Unfortunately, modeling drift has not been measured in most circumstances and its variation is largely unknown. Moreover, effects of growth, modeling, and drift can be difficult to differentiate quantitatively. The general challenge of accurately visualizing formation phases or quantifying drift has limited our understanding of bone modeling histomorphology, in contrast to remodeling, which leaves behind osteons as obvious features of its activity.

A proposed solution has been to use the drifted endocortex as an indicator and summary of net modeling drift (Maggiano et al. 2011). In fact, this drifted endocortical bone is so predictably located and histomorphologically distinct (Fig. 1), it has been treated as its own microstructural meta-feature, called the endosteal lamellar pocket (ELP), and has several possible applications in bioarchaeological and forensic contexts (Maggiano et al. 2011, 2013; Maggiano, 2012b; Raguin et al. 2014). The ELP is characterized by hemicircumferential primary lamellae deposited in continuous series or stratigraphic phases to one side of the medullary cavity. Depending on the individual's age, its oldest layers can agree with a much smaller partial circumference, having been formed by a smaller medullary cavity in childhood and can be relatively devoid of osteons due either to its internal position away from the largest strains initiating targeted remodeling or perhaps to its differing strength. Whereas human primary periosteal tissue entombs almost exclusively longitudinal vessels, the ELP is instead vascularized by radially oriented primary Volkmann's canals, reaching from the medullary cavity deep into the bone and providing the basic void structure for the first invading osteons of the feature. The youngest layers of the ELP (formed when the individual was older) are on the surface of the cavity while the oldest childhood tissues are deep in the intercortex. Sometimes these earliest layers directly abut periosteal tissues formed after drift had ceased but diametric growth had not, in other younger individuals the ELP itself comprises the entire cortex on the lagging side of drift with the external cortical tissue being endosteal in origin. By observing microscopic bone modeling at this macroscopic scale, structural variability in the drifted cortex can be interpreted rather than avoided. A large part of the current methodological development and comparison arises from the recognition that the ELP offers new variables for comparing growth and mechanically adaptive responses in bone that transpire over many years of an individual's life for many types of bone investigations.

Methods

Sample selection and preparation

The current study focuses on a pooled sample of modern and archaeological remains: the modern mortuary sample comprised unidentified or unclaimed remains recovered from the Xoclan cemetery in Merida, Mexico (for more detailed information see Chi-

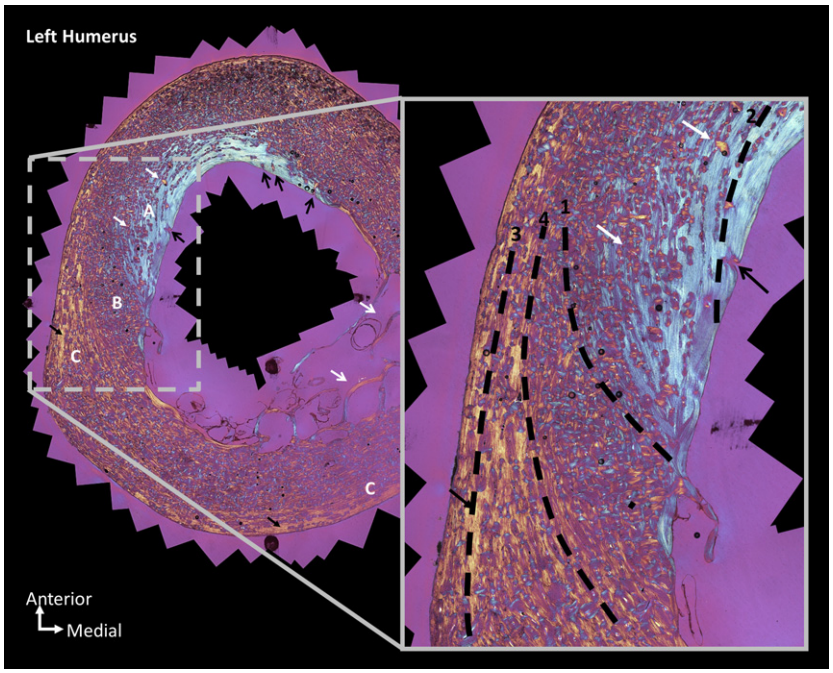

Fig. 1 Micrograph of a complete humeral cross-section generated using digital stitching in Autopano Giga®. Each image was captured using a 530-nm compensated, cross-polarized 45° photographic technique, augmenting the primary tissue contrast and orientation. In this illustrative image the endosteal lamellar pocket (ELP) (A) was photographed with lamellar bone at one 45° angle, rendering it blue; Haversian tissue (B) show up 'mottled', displaying both warm and cool hues; periosteal tissue (C) was photographed at the other 45° angle, lending it a golden hue. Black-lined arrows denote large, radially oriented 'primary Volkmann's' canals responsible for initial vascular supply of endosteal tissue. White solid arrows mark secondary remodeling events or osteons beginning to reorganize ELP primary tissue, and black solid arrows show the same in periosteal tissue. Unlike the endocortex, the pericortex has a primary vascularization that is longitudinal (made up of primary canals, sometimes called primary osteons if they contain lamellae). White-lined arrows mark trabecularization of once highly remodeled periosteal origin compact tissue. These features combined, along with the position of the ELP, indicate the repositioning of the medullary cavity due to a net posteromedial drift. The insert details differences in orientation between old (i) and more recent (ii) endocortex, and old (iii) and more recent (iv) pericortex. Left humerus from the Xoclan cemetery, Merida, Mexico, male 35 years old at death. Unlike this illustrative image, analytical imaging for this project did not photograph endosteal and periosteal bone at different angles (in those images, all primary tissue was blue vs. mottled secondary tissues).

Keb et al. 2013), as well as remains recovered from the nearby Xcambó archaeological site (AD 350–700).

Both skeletal collections are the current focus of a larger project investigating human bone histomorphological variation between ancient and modern populations from the region. For this reason, skeletal material from this collection was available for thin-sectioning necessary for microscopic visualization and quantification of tissue distributions. After the removal of individuals with obvious lesions, healed fractures or poor preservation, the combined sample included the remains of 73 adults and juveniles within the target age range of 4.5–65 (Table 1). Males and females were approximately equally represented. Individuals lacking a significant endosteal deposit could not be included for measurement, reducing the total sample to 58 for the current study (an ELP prevalence of 74%). It is unclear what total populational variability exists in the ELP prevalence, if any; however, in nearly all cases, individuals lacking this drift remnant were assigned to the oldest ages represented in the group (with only four falling below 50). The current study pools all subsamples in order to include younger individuals typically not present in modern collections and to maximize variability in tissue distributions.

The target age range was limited to exclude individuals who did not yet have a mature walking gate and those who had lost significant amounts of bone from age-associated osteopenia or osteoporosis. Humeral elements were of primary interest due to their relatively decreased cortical area compared with femora, which permitted more rapid analysis. In addition, tissue distributions in the humerus are less well characterized in the bone histomorphometric literature, ensuring the value of collected data for continued investigations in growth and biomechanical adaptation.

Table 1 ELP presence and age profiles for pooled sample (n = 17 Xoclan, 56 Xcambó).

	Individuals	Age range*	Average age*
Without ELP	15	30–65	49.3
With ELP	58	4.5–65	28.6
Total	73	4.5–65	33.2

*Xoclan documentation included known-age, multivariate techniques used to estimate age at Xcambó are outlined in detail in Maggiano et al. (2008b).

After macroscopic osteometric data had been collected, the anterior and proximal aspects of the midshaft region were marked. Both epiphyseal and local diaphyseal landmarks were used to determine the anterior–posterior axis (the line best summarizing the positions

of the lesser tubercle, the most superior aspect of the brachialis insertion, and the apex of the anterior curve between the lateral and medial supracondylar crests). Transverse excisions of 2 cm were taken using a handsaw and were prepared as suggested by Schultz & Drommer (1983) and Schultz (1988). All information on anatomical orientation was preserved throughout the process of thin-ground section preparation and subsequent reconstruction (Maggiano, 2012a).

Starburst point-count sampling

Microscopic slides were prepared for the starburst technique by marking the cross-sectional centroid and eight ROIs reference points on the glass with permanent marker. For this, the slides were simply overlaid on scale-matched prints of optical scans that had been geometrically analyzed in ImageJ® [using MomentMacroJ v1.4, public net access courtesy of Ruff] to locate the centroid. Finally, a glass platform was constructed on top of the stage to satisfy requirements for sample mobility without eliminating x/y tracking; a standard circular stage with an x/y slide mount was time-limiting and could not track sufficiently for larger cross-sections.

The microscope used for this investigation was a wide-field standard optical Olympus® microscope, model BX51 (Olympus America, Inc., Center Valley, PA, USA). Basic digital imaging was accomplished using the Spot Idea CMOS 3.0Mp camera system and Spot Advanced® software and a 64-bit Desktop with 6 GB of RAM. Cross-polarized light compensated at 530 nm (Olympus U-TP530 nm) was used to aid in discerning fragments and lamellar orientation and for consistency with the hand-drawn method.

Point-count histomorphometry involves the aid of a counting reticule integrated into one of the oculars, providing set points at grid intersections where identifications or counts can be made of differing tissue types or features. For simplicity, hereafter, 'field of view' (FOV) will refer to the area within the 36-intersection grid of the reticule. Specifically, a sine patterned Merz Grid (Merz & Schenk, 1970) was used in this study, superimposed on the tissue at each region of interest (ROI) at 100× total magnification. A more detailed methodology, including guides for terminology, counting parameters, and differentiating tissue types and void spaces, is available elsewhere (Maggiano, 2012a,b).

Many different sampling schemes have been employed in bone histomorphometric studies to select which FOVs to count in what ROIs, largely because of the time intensiveness of the point-count process (see Iwaniec et al. 1998 for a quick reference with schematics for several studies). The choice of sampling structure depends on the level of desired predictability and the time available for the analysis (Iwaniec et al. 1998), which increases with the total sample area and number of counted variables per FOV. The potential for counting and transcription errors during data collection can also be an issue, especially with the large number of counted variables used in the wider project. For these reasons, a novel point-count sampling method was employed along with custom software for data entry that permitted both more rapid analysis and the preservation of their spatial relationships for later use.

The basic sampling effort in this study is similar to that employed by Robling & Stout (2003), but has been modified to more accurately discern directionality in tissue distributions (Fig. 2A) by using a novel 'starburst' point-count technique to sample a single transcortical track of FOVs in each of eight ROIs (anterior, anterolateral, lateral, posterolateral, posterior, posteromedial, medial, and anteromedial), each intersecting at the calculated centroid of the bone and radiating to the outer cortex (Maggiano et al. 2009). In this way, the starburst point-count pattern offers a standard sampling of total count (number of occurrences per FOV), point-count (occurrences at each grid intersection), and area data (percentage of total hits) in distributed tissues, and does so along four potential bending axes, providing histomorphometric data easily relatable to cross-sectional geometric or biomechanical contexts.

The distributed area for each tissue of interest was calculated by standardizing its number of hits by the total 'on bone' hits counted in the cross-section. To quantify the position of that distribution relative to the rest of the cross-section, endosteal (or periosteal) hits per ROI were then used to weight each ROI angle (at each 45° interval), constructing a summary vector with a single angular measurement in degrees (as per Zar, 2010). The reference angle chosen was lateral, relative to the posterior ray of the cross-section (Fig. 2A).

Hand-drawn endocortical histomorphometry

Outlining regions of tissue variability or type has become a useful tool for discussing cortical growth patterns (Goldman et al. 2009), and has here been modified to reflect a focused interest on the distribution of endosteal origin tissues as an indicator of bone modeling drift for comparison with the point-count method. This study targets the endocortex rather than pericortex due to the conflating local and systemic influences determining periosteal bone deposition and the potential confusion between local morphology and larger scale drifts. Endocortical drift effects the repositioning of the medullary cavity with respect to the net result of adaptive and growth inputs on bone morphology, summarizing the net modeling drift of the long bone at a given transectional plane (Maggiano

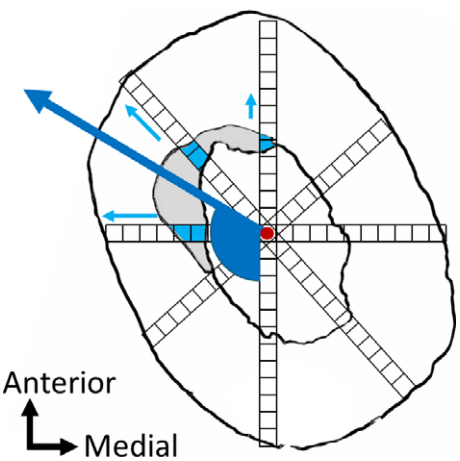

Fig. 2 Schematic representation of the starburst sampling pattern superimposed on a left humerus. Four sampling axes construct eight regions of interest (ROIs) corresponding to the anterior, anterolateral, lateral, posterolateral, posterior, posteromedial, medial, and anteromedial aspects of the cross-section. Counts were made from the outside field of view (FOV), inward. This array increases the likelihood of sampling distributed tissues in biomechanically informative axes while keeping efficient total times of analysis. Endosteal sampled area shown in dark-shaded FOVs. Endosteal hits there weighted a vector (large arrow), defining the point-count ELP position as the angular deviation from the posterior ROI.

et al. 2011). For this reason, primary periosteal tissue was not hand-drawn.

To hand-draw endosteal primary tissue with great accuracy, several requirements must be met: (i) high enough the magnification and contrast to permit distinguishing primary and secondary tissues, and tissues of periosteal and endosteal origin, (ii) wide enough FOVs to relate the entire ELP to the geometry of the total cross-section. These goals can be achieved through the use of digitally merged micrographs constructed with photo stitching software, combined with custom polarized microphotography. Increasing tissue contrast between primary and secondary tissue was accomplished using cross-polarization. This technique, however, produces a 'Maltese cross' darkening artifact in circular, layered birefringent structures, such as osteons, and becomes problematic when photographing primary bone which also contains circumferential or hemicircumferential lamellae, sometimes leading to the darkening of several square centimeters of tissue (Fig. 3).

Although other forms of polarized light (such as circular polarization) circumvent the inclusion of this artifact, in this case this could be an advantage. This was accomplished through the development of a 45° image acquisition protocol which ensured, via constant manipulation of the orientation of the slide, that primary tissues were only photographed in one 45° axis relative to the stage. The result is a stitched image of the cross-section which represents primary tissue photographed only when at maximum brightness and lacking any cross-polarization interference artifacts. In contrast, Haversian systems had their entire circumference photographed in each of these low magnification images and were therefore darkened by their Maltese crosses. Finally, to even further separate and distinguish primary bone structure, red-quartz compensation (530 nm as discussed previously) was used to differentially color the bright field in the polarized image, depending on tissue orientation: cool hues for one 45° orientation, warm hues for the other. Therefore, in addition to appearing darker from the interference artifact, each osteon also displayed all the colors added by the compensator, whereas primary tissue photographed at only one 45° orientation was accentuated by a single bright hue due to its much larger scale of curvature (Figs 1 and 4A). Stitching these images required software capable of robust merging and color-balancing functions. Collected images were at odd angles relative to one another and contained different colors for the same tissue in their overlapping regions. Unlike many other available image editing programs, Autopano Giga® (by Kolor®) is capable of performing rapid stitching under these conditions and also offers batched rendering functions and quantification of control point matches.

Photoshop CS5.1® was used to outline endosteal tissue constituting the ELP under digital zoom. To reduce the time investment in hand-drawing the endosteal tissue, a lower threshold for inclusion in the drawn area was set at the size of the diameter of an average osteon (roughly 200–300 μm). If a region in the outline had a minimum width below this threshold and did not appreciably increase thereafter, then this point would define the boundary of the outlined area. Outlines were then saved as images and had their centroids assigned by the same ImageJ process used on the total cortical area. The ELP centroid was then used as the summary for the distribution of endosteal tissue relative to the cross-sectional centroid. A composite file was made using Photoshop layering (Fig. 4A) which included: (i) the cross-sectional scan, centroid, geometric axes; (ii) the stitched ELP micrograph, outline map, and centroid; and (iii) a total cross-sectional stitched micrograph with rough designations for all tissue types and accompanying notes. Scales and orientations were adjusted and confirmed using the complete cross-section micrograph as a semi-transparent template. This composite allowed the simultaneous consideration of cross-sectional geometric and hand-drawn tissue distributions. At this point, the cross-sectional centroid and ELP centroid were connected by a line, defining the angular position of the ELP laterally, relative to the marked posterior ray on the slide (Fig. 4B). The direction opposite this line was the quantified linear drift direction for the cross-section.

Analytical methods

Data collected from each method were applied to two major inquiries: (i) whether both methods are similar in their reports on ELP position, and (ii) whether both methods are similar in their reports on ELP size. Angles derived by the point-count and hand-drawn methods were compared using techniques developed for generating and comparing angular means (Zar, 2010) due to the equivalence of 360° and 0°, a violation of linear statistical assumptions. After these vectors were constructed for periosteal and endosteal primary tissue distributions (endosteal point-count angle, or PEAn; periosteal point-count angle, or PPAn), they were plotted against the ELP centroid determined angle determined from the hand-drawn data (endosteal hand-drawn angle, or HEAn). PPAn is reported here to test the comparative usefulness of periosteal tissue distributions to indicate drift. If PEAn is similar to PPAn + 180°, then

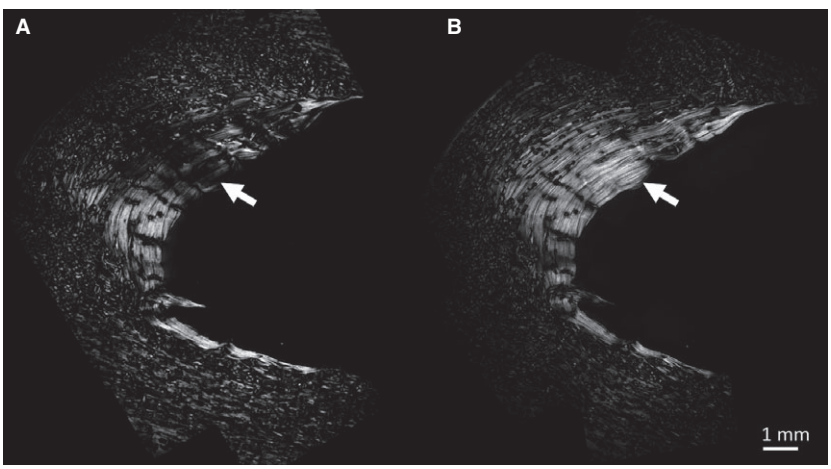

Fig. 3 (A) Right-angle stitched micrograph demonstrating the interference artifact typically discussed in secondary osteons, the 'Maltese cross' artifact, disrupts visibility of tissue even more dramatically in primary tissue. (B) Using the 45° stitching technique, however, ensures primary tissue is only photographed at its brightest orientation. Upon reconstruction, the artifact is absent from the primary tissue, but is importantly retained in secondary tissue due its much smaller diameter. This has the combined effect of increasing visibility of primary tissue in whole cross-section microphotography. Scale bar: 1 mm.

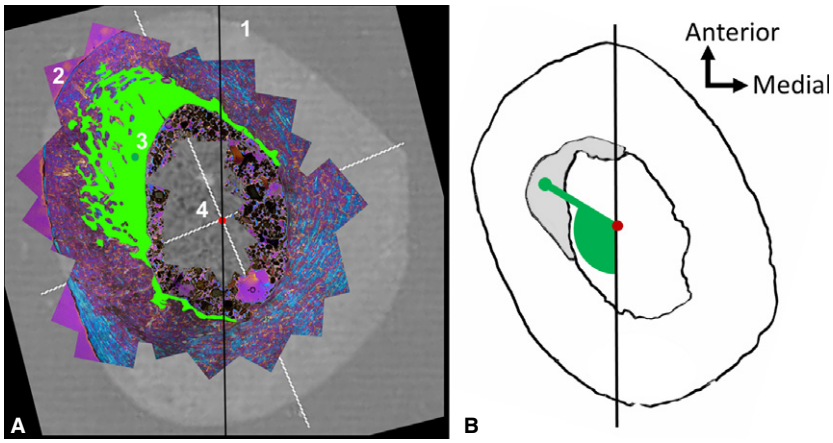

Fig. 4 (A) Overlay generated to permit the geometric measurement of drift histology, including: (i) the total cross-sectional scan, (ii) the 45° stitched cross-polarized micrograph, (iii) the hand-drawn mask defining the ELP and its centroid, (iv) the ImageJ generated geometric data including the cross-sectional centroid (~7-year-old left humerus from an individual from Xcambó). (B) Schematic representing the angle recording ELP position (HEAn), defined in degrees deviation between the posterior aspect and the line connecting both centroids.

Table 2 Descriptive statistics on tissue distributions (position and size) as assessed by point-count and hand-drawn techniques.

	Point-count endosteal			Point-count periosteal			Hand-drawn endosteal		
	Range	Mean	SD	Range	Mean	SD	Range	Mean	SD
Mean angle (°)	184*	144.8	38.3	126*	336.1	27.7	181*	141	38.3
Mean area (%)	0.2–0.47	0.145**	0.118				0.1–0.39	0.096***	0.096

*Degrees about the mean.
**Standardized by total cortical hits per individual.
***Standardized by total cortical area.

both tissues indicate the same general linear drift direction. All angular measures were compared using Moore's non-parametric paired-sample test for circular means (Zar, 2010), since Hotelling's test requires Von Mises distribution, analogous to the linear normal distribution. A combination of SPSS® 19 and Oriana Circular Statistics® 4 was used for all analyses performed.

Point-counted endosteal area (PEAr) was determined by adding the total endosteal hits and standardizing by total cortical bone hits for each FOV, ROI, and individual. Likewise, the hand-drawn endosteal area (HEAr) was determined through image analysis and standardized by total cortical area determined by Moment Macro and ImageJ (Ruff). Statistical comparison of PEAr and HEAr was accomplished using the Wilcoxon ranked-sum test for paired data with non-normal distributions. To use this test, it was necessary to confirm three assumptions: (i) each observation pair was from a random sample and was independent from other pairs; (ii) the sample size was relatively large (much greater than the suggested minimum of 16 pairs); and (iii) the distribution of differences scores was continuous and symmetrical (Green & Salkind, 2008).

Results

The point-count and hand-drawn techniques both returned effective data on cortical tissue type distributions (Table 2). At peak efficiency, each method took roughly 3–4 h per sample for data collection. Adjustment of raw values and preparation of data were much slower using the point-count technique than hand-drawing. Overall, hand-drawing typically took half the time point-counting did, because the generation of results from drawings, including overlay construction and image analysis, was greatly facilitated by batch processing and the use of Photoshop macros.

Results indicate that ELP position as measured using endosteal point-count angle (PEAn) and endosteal hand-drawn angle (HEAn) were similar. PEAn was positioned anterolaterally with a range of 184° about a mean of 145° ± 38.3 from the posterior aspect of the cross-section (Fig. 5), and HEAn results were similar, with a range of 181° about a mean of 141° ± 38.3. Both of these measures indicate a general posteromedial drift in the humerus that is both obvious and statistically significant according to a Moore's modified Rayleigh's test for uniform circular distributions ($P < 0.001$ at $\alpha = 0.05$ for all tissue types). Pairwise comparisons show similarity between reported angles, and the results of a Moore's test of paired circular means supports the hypothesis that there is no difference in position assessment provided by the custom point-count and hand-drawn techniques ($R' = 0.361$, well under the test limit $R'_{\alpha=0.05,\ n=50}$, 1.007).

Point-count periosteal angles (PPAn) show less variation in position than endocortical measurements determined by either method. In addition, the angular positions of the periosteal and endosteal bone are often counterposed on either side of the cross-section, indicating roughly the same drift direction. However, pericortical and endocortical

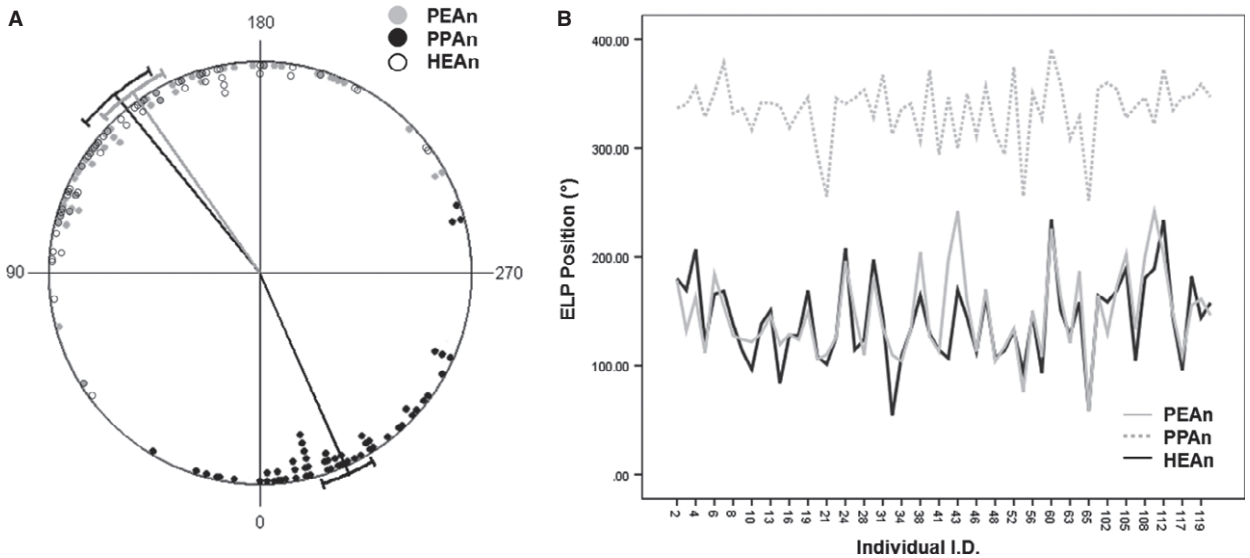

Fig. 5 (A) Circular distribution of point-count endosteal and periosteal angles (PEAn and PPAn) and hand-drawn endosteal angles (HEAn), as well as their means, and standard deviation. Note the predictable general position of the ELP in the anterolateral aspect of the cross-section and the near direct opposition of periosteal tissue (which has a slightly smaller range and is less variable). (B) The same data plotted for pairwise comparisons shows that both techniques identify similar trends in ELP position, despite a few differences approaching 50°.

indications of drift, compared by adding 180° to the former, are significantly different (PPAn vs. PEAn, $R' = 1.781$; and PPAn vs. HEAn, $R' = 1.651$, according to Moore's Test).

The area occupied by the ELP was more variable, averaging 10–12% of the cortex in most individuals but accounting for nearly half of the total cortical area in others. Pairwise comparisons of endosteal lamellar area (as a percentage of total cortical area) indicate that although both techniques identify the same trends in ELP size, the hand-drawn endosteal area (HEAr) was larger than the point-count measure (PEAr) (Fig. 6). The results of a Wilcoxon ranked sum analysis support the hypothesis that this difference is statistically significant ($P = 0.00$, $\alpha = 0.05$).

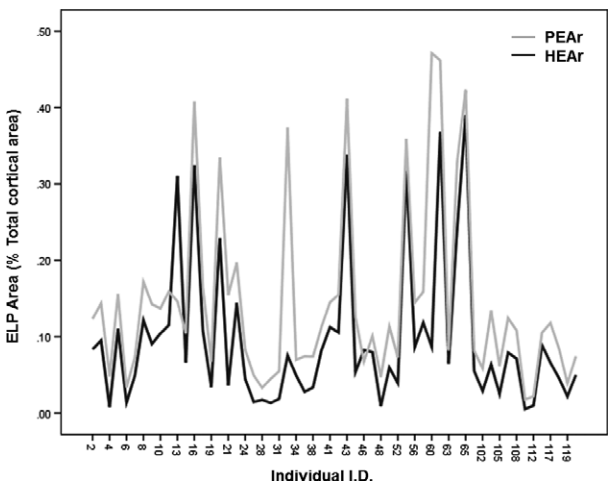

Fig. 6 Pairwise comparisons of endosteal lamellar area shows that although reporting the same trends, PEAr and HEAr, as measured in this study, do not equally report endosteal area.

Discussion

Recently, there has been a resurgence of interest in primary bone histology (Herrmann & Danielmeyer, 1994; Castanet et al. 1996; Skedros et al. 2001; De Margerie, 2002; De Margerie 2002b; De Margerie et al. 2002, 2004; Castanet et al. 2004; Skedros & Hunt, 2004; Castanet, 2006; Bromage et al. 2009; Goldman et al. 2009, 2014; Maggiano et al. 2011; Cambra-Moo et al. 2012, 2014; Maggiano, 2012a; Raguin et al. 2014) and in the way it affects distributions of secondary tissue (Paine & Godfrey, 1997; McFarlin et al. 2008). Studies on regional distributions of cortical tissues generally find high degrees of microstructural variability (Jowsey, 1966; Pfeiffer et al. 1995; Goldman et al. 2003a,b, 2005, 2009; McFarlin et al. 2008). Due to the highly invasive nature of vital staining and optical microscopy, most of these studies do not use experimental fluorescent labeling (for important exceptions see Newell-Morris & Sirianni, 1982; Castanet et al. 2004; Bromage et al. 2009) and are therefore more applicable to analysis of human bone, whether modern or archaeological. However, completely characterizing and comparing modeling drift in long bone diaphyses requires new replicable, quantitative techniques and would be facilitated by the recognition of modeling drift BSUs.

Our initial assessment of femora from a similar population sample (Maggiano et al. 2008a, 2011) suggested that the cross-sectional distribution of endosteally deposited

tissue is itself a modeling BSU satisfying that requirement, one we referred to as the endosteal lamellar pocket (ELP). The ELP was considered a modeling meta-feature sufficiently prevalent, predictable, and discernible for use as a drift summary. This is because, unlike any other BSU, it records the net movement of the medullary cavity through tissue-space-time, at least until early adulthood (Maggiano, 2012a). The potential for this meta-feature to summarize drift has been borne out by the current study which includes a larger sample size and corroborates original observations on the ELP using two different methods. Identifying histological features of the ELP include hemi-circumferential lamellar formation phases that are incongruous with the general circumferential phases (either periosteal or endosteal), reduced relative osteonal presence compared with other inner cortical regions, and radially oriented 'primary Volkmann's canals' not common in other tissues (Maggiano et al. 2011; Maggiano, 2012b). In a previous study, observed ELP prevalence was 84% in the femur (Maggiano et al. 2011). Here, however, the 74% humeral prevalence cannot be directly compared, as it includes both a larger sample and greater proportion of older individuals. In nearly all cases, individuals missing ELPs were older (> 45 years estimated or actual age). This is expected due to both the proliferation of osteons (intracortical remodeling of the ELP margin) and the expansion of the medullary cavity (endosteal surface resorption and intracortical resorptive bays with increasing age) (Maggiano, 2012a). Our observations have shown ELPs in individuals roughly 60 years old. It is important to note, however, that even older individuals (70–90 years old) occasionally retain this feature or at least remnants of it (Gocha & Agnew, 2014). However, Cambra-Moo et al. (2014) recently recorded a much lower prevalence of endosteal deposition than would be expected given the current study and considering that well over half of their sample consists of subadults. Although it was not the focus of study, their presented raw data seem to indicate that only nine of 15 individuals (a 60% prevalence) had significant endosteal tissues. Part of the discrepancy is likely introduced by their sample's small representation of children (seven of nine subadults were pre-ambulatory), which raises interesting possibilities for considering the complexities of growth and biomechanical influences on modeling drift. The current study did not include pre-ambulatory subadults and also differs in that it excluded individuals that displayed morphologically insignificant amounts of endosteal tissue on the basis of having no ELP. For all these reasons, larger population samples and various (sub-)populations will need to be examined before total ELP prevalence and variance is completely understood.

Drift direction defined by tissue distributions

Results of both techniques reveal a posteromedial drift in the human humeral midshaft with roughly equal posterior and medial variances. Although, to our knowledge, the current study is the first to observe and quantify the human humeral drift direction, the general trend has been observed in other studies on non-human primates (also see Cambra-Moo et al. 2014 for corroborating images in their mineralization and tissue-distribution study). McFarlin et al. (2008) identified a posteromedial drift in their histomorphological assessment of catarrhine primate humeri (especially those of *Chlorocebus aethiops*), and note that Newell-Morris & Sirianni (1982) report a similar observation in the fetal pig-tailed macaque. Since the anterolateral to posteromedial axis is responsible for resisting the combined effects of shoulder abduction and flexion (Aiello & Dean, 2002; Moore et al. 2011), the ELP may provide a measure of relative dominance of one or the other of these upper arm movements. If confirmed through further testing, this observation could be employed to resolve questions about locomotion, or other elements of upper body biomechanics, and factor into developmental or adaptive interpretations of carrying angle, humeral torsion, or even activity reconstruction in bioarchaeological contexts.

We originally postulated that both growth and local mechanical adaptation could obscure periosteal indications of drift. The data presented here seem to provide some support for this suspicion, since endosteal and periosteal indications of drift were found to be significantly different. Unexpectedly, however, PEAn provided slightly lower variance in its assessment of drift direction, demonstrating that further study is necessary before it can be decided whether its inclusion diminishes the precision of the ELP drift summary or enhances it. Several lines of additional evidence, however, support the working hypothesis that the ELP, when present, provides a better summary for drift than the total distribution of periosteal tissues:

1 Its position in the interior of the cortex seems to protect its most recent phases from conversion to secondary osteonal bone by targeting remodeling more common in higher strain exterior cortices (Biewener, 1992).
2 There exists a general consensus that the endosteum shows reduced or nonexistent responses to the general mechanical loading of the element relative to the periosteum (Meade et al. 1984; Jones et al. 1991; Gross et al. 2002; Lee et al. 2002; Srinivasan et al. 2002), and therefore would more accurately summarize the element's net drift.
3 Diametric growth decreases the directional signal the drift-deposited pericortex might otherwise provide.
4 Endosteally deposited bone is free from potential soft tissue impediments to local deposition, such as muscle bellies (Carpenter & Carter, 2008), arteries or entheses that have a direct effect only on periosteal activity. There are aspects of drift, however, that the current study has not yet resolved.

Nearly all individuals displaying an ELP showed some evidence of curvilinear drift, as described in detail elsewhere (Maggiano, 2012a). In general, humeral ELPs consist of many phases of endosteal bone formation, each often deposited at a slightly different relative orientation to the last. This stepwise process results in a pivot point in the feature (typically in the posterior or lateral aspect of the humeral ELP) that marks an obvious rotational drift. Rotational drift is oriented clockwise in the left element and counterclockwise in the right, suggesting that the earliest phases of drift are more medial and later phases more posterior. Unfortunately, the techniques tested here do not permit the quantitative assessment of curvilinear drift, and its interpretation awaits continued research and method development.

Primary tissue distributions by area

Results from this study suggest that as much as 45% of the total cortical area may be endosteal in origin, with a significant portion of that tissue sometimes in the outer third of the cortex. Although Cambra-Moo et al. (2012, 2014) did not measure or report the position of endosteal bone in detail, they did quantify its area in six individuals. Their raw data suggest endosteal bone made up 12.1% of the total cortex, a value that is consistent with the 10–15% (hand-drawn ELP to point-count endosteal measurements, respectively) reported here. Interestingly, recent work by Raguin et al. (2014) focusing on the second metacarpal also found that the ELP constitutes roughly 12.5% of the total cortical area.

Implications for the consistent deposition of significant amounts of endosteal tissue during cortical drift are broad. Endosteal bone remnants, maintained well into late adulthood, offer new potential for improving many aspects of regional histomorphometric analysis, from age-estimation, osteon typologies, and micro-crack counts, to mineralization, vital labeling, and vascularization assessments. The work of Goldman et al. (2005, 2009) and McFarlin et al. (2008) accurately incorporates modeling drift into their interpretations and demonstrates some of the limitations of separating the cortex arbitrarily into inner, middle, and outer thirds. This sampling strategy is likely to over-inflate assessments of variation in cortical microstructure and could obscure statistical relevance of regional comparisons for many types of data. McFarlin et al. (2008) use a detailed consideration of modeling drift theory to explain deviations from their expectations regarding Haversian tissue distributions. Likewise, Goldman's research group has also successfully turned to modeling drift assessment (2009) as a means of explaining some of the substantial variation they recorded in collagen orientation and mineralization in femora (Goldman et al. 2003a,b, 2005). In general, this growing body of work, recognizing that exterior tissue can be interior in origin, also cautions against the use of the terms 'peri'- or 'endo-cortex' to describe regions rather than tissue origins (Maggiano, 2012b). It is this type of change in perspective, favoring the use of primary tissue distributions to better compare and understand other elements of bone anatomy, including cross-sectional geometry and histology, that will answer long-standing questions about differential effects of growth, physical adaptation, injury, and disease in bone.

Comparing the techniques

The current research tests two techniques adapted to the relatively new goal of quantifying cortical drift from diaphyseal transections: a starburst-modified point-count, and hand-drawings from 45° cross-polarized stitches. Results of these two techniques were largely complementary, particularly in their ability to discern the position of distributed tissues, like the ELP. To this end, either technique could be used to analyze drift and compare individuals and subpopulations. It is our opinion that the starburst point-count technique is more versatile, however, and offers considerable advantages over hand-drawing. These include simultaneous collection of traditional histomorphometric variables (with a total area of data collection similar to Robling and Stout's technique in 2003, and abiding by Iwaniec et al.'s (1998) advice on collecting 'representative' histological data), and the possibility for correlating results with cross-sectional geometric data.

Unfortunately, the starburst point-count technique provides no means of assessing curvilinear drift, or the orientation of primary formation, arrest, or reversal phases. In addition, despite the standardization of area values by total cortical area, inner tissues are more representatively sampled than outer tissues. To some degree, disproportionate representation of histological features is an unavoidable side-effect of sampling bone, due both to the nature of circularly distributed features and to the comparably stable size relative to total cortical area.

Whereas the starburst point-count method was created to satisfy many objectives simultaneously, the hand-drawn technique was meant to offer a quicker means of drift assessment. In part, this is one of the reasons it did not include the drawing of all endosteal tissues. The internal lamina was excluded for time efficiency, but also because it is more likely to be the result of 'secondary modeling' (or secondary remodeling, via hemiosteons), a process that seems to maintain the endocortical surface well into adulthood. This element of experimental design explains the discrepancy between compared techniques in the assessment of 'ELP area', one expected to be negligible.

In comparison with the technique used by Goldman et al. (2009), where assessment of formation or resorption on *perimortem* cortical surfaces is used to determine general drift direction, techniques presented here offer several advantages: (i) they can be performed on individuals of

any age, whereas surface analysis requires that the cortex be active in a growing individual; (ii) they can be performed on individuals from archaeological or forensic contexts where the cortex is sometimes too damaged to identify Howship's lacunae or *perimortem* lamellar phases, and most importantly, (iii) they permit a future focus on ELP morphology and biostratigraphy indicating changing orientation, arrest, or reversal of primary formation phases. Some of these benefits (i and ii) are also found in the ELP thickness measurement technique employed by Raguin et al. (2014), who investigated the second metacarpal, which is likely the quickest technique for assessing drift direction. The Geographical Information System (GIS) technique provided by Cambra-Moo et al. (2014) offers some advantages over the multi-imaging process used here for more complex spatial analyses; however, the significant time and data management required to analyze several compact tissue types with GIS could pose a challenge. The elegant method applied by Raguin et al. (2014) serves as a reminder that even the macroscopic quantification of microscopic detail does not always require complex image analysis. Part of the benefit of detailed efforts to increase tissue distinction (through cross-polarization quartz compensation and 45° stitching) lends itself well to improvement of the accuracy of automatic tissue recognition. Such a technique is not yet available but is a goal of future work.

Conclusion

Results of this study demonstrate that hand-drawn and point-count techniques provide similar information regarding drift direction and total area of endosteal tissue, independently corroborating findings from prior work and encouraging the burgeoning interest in primary bone histomorphology in anatomical and bioarchaeological contexts. These results support the working hypothesis that the endosteal lamellar pocket functions as a bone structural unit of modeling drift within a fairly broad time-span of juvenile and young adult life, summarizing net diaphyseal growth and adaptation as the medullary cavity repositions itself within the periosteal cortex. In some cases, over a third of the diaphyseal transection consists of endosteal origin bone, and its distribution can reach the exterior margins of the cortex. The endosteum is not simply a resorptive membrane as is sometimes assumed. Instead, it is nearly as osteogenic as the periosteum, performing important resorption and formation during the achievement of biomechanically adaptive adult morphology, and leaving traces behind well into the 6th and 7th decade of life. Humeral drift proceeds in a net posteromedial direction, with a tendency toward posterior rotation. In the humerus, this drift axis is consistent biomechanically with elongation in resistance to deltoid and brachialis activity. Future research will illuminate the relationship between drift and the differential involvement of these and other humeral mobilizers during physical activity.

In comparing the two techniques used to measure drift in this study, the starburst point-count technique is found to be advantageous for simultaneous collection of multiple count variables per field of view or region of interest. The hand-drawn technique is more rapid and permits the future collection of curvilinear drift and primary arrest and reversal line data. Although potentially even more rapid techniques exist (Raguin et al. 2014), the hand-drawn technique lends itself readily to advanced geometric morphometric analyses planned for later studies. Additional efforts will test 45° cross-polarization and quartz compensated imaging for its ability to facilitate automatic tissue recognition. More detailed demographic and biomechanical analyses of humeral and femoral drift are also underway for the population samples used in this study.

The continued investigation of diaphyseal modeling drift has the potential to improve many efforts that rely on bone histomorphology, regardless of the field of inquiry. Comparisons of histological features or material qualities by region will benefit from considering the overall drift model for the element, or even specific drift-defined zones indicating relative tissue age-at-formation. In this way, even without vital labeling, it is possible to avoid false comparisons between tissues of the same region but differing tissue-ages or membranes of origin. Specifically, these types of considerations could improve histological assessment of biological age and distributional analyses of osteocytic lacunae, microfracture, osteon types, vascularity or porosity, and improve sampling site protocols for stable isotopic and other chemical analyses. An understanding of bone growth and mechanical adaptation is incomplete without accurate means of assessing modeling drift. Continued efforts will ensure that techniques such as these are optimized to permit observation, quantification, and statistical comparisons of drift between elements and individuals toward new applications in skeletal sciences.

Acknowledgements

This project was funded by the National Science Foundation (DDIG #1061169), the Mexican CONACYT (Grant 49982), and the Deutsche Forschungsgemeinschaft (MA 4702/1-1), Germany. The bone sections were processed and prepared for microscopic analysis at the Department for Anthropological Sciences, Universidad Autónoma de Yucatán, Merida, Mexico. The work on the archaeological specimens from the site of Xcambó, Yucatán are part of a collaboration with Dr. Thelma Sierra, whose role we hereby thankfully acknowledge. The study of the archaeological specimens was authorized by the Consejo de Arqueología/INAH. The sampling of the documented reference series from the Xoclán Cemetery of Merida was possible thanks to an agreement with the Municipal Government of Merida and the support we received from the personnel of the Xoclán Cemetery. We wish to thank local students in Merida for their help and assistance during sample preparation and the restoration of sectioned bone segments. Analyses were undertaken

at the Department of Anthropology, Ohio State University. We thank Petra Creamer and Anne Jordan for their help during analysis. We are also grateful for the thoughtful conversation and constructive advice of colleagues and past contributors Michael Schultz and Margaret Streeter.

References

Aiello L, Dean C (2002) *An Introduction to Human Evolutionary Anatomy*. New York: Academic Press.

Biewener A (1992) *Biomechanics – Structures and Systems*. Oxford: Oxford University Press.

Bromage TG, Lacruz RS, Hogg R, et al. (2009) Lamellar bone is an incremental tissue reconciling enamel rhythms, body size, and organismal life history. *Calcif Tissue Int* **84**, 388–404.

Cambra-Moo O, Nacarino Meneses C, Ángel Rodríguez Barbero M, et al. (2012) Mapping human long bone compartmentalisation during ontogeny: a new methodological approach. *J Struct Biol* **178**, 338–349.

Cambra-Moo O, Nacarino Meneses C, Ángel Rodríguez Barbero M, et al. (2014) An approach to the histomorphological and histochemical variations of the humerus cortical bone through human ontogeny. *J Anat* **224**, 634–646.

Carpenter RD, Carter DR (2008) The mechanobiological effects of periosteal surface loads. *Biomech Model Mechanobiol* **7**, 227–242.

Castanet J, Grandin A, Abourachid A, et al. (1996) Expression de la dynamique de croissance dans la structure de l'os periostique chez *Anas platyrhyncos*. *C R Acad Sci III* **319**, 301–308.

Castanet J, Croci S, Aujard F, et al. (2004) Lines of arrested growth in bone and age estimation in a small primate: *Microcebus murinus*. *J Zool* **263**, 31–39.

Castanet J (2006) Time recording in bone microstructures of endothermic animals; functional relationships. *CR Palevol* **5**, 629–636.

Chi-Keb JR, Albertos-González VM, Ortega-Munoz A, et al. (2013) A new reference collection of documented human skeletons from Mérida, Yucatan, Mexico. *Homo* **64**, 366–376.

De Margerie E (2002) Laminar bone as an adaptation to torsional loads in flapping flight. *J Anat* **201**, 521–526.

De Margerie E, Cubo J, Castenet J (2002) Bone typology and growth rate: testing and quantifying 'Amprino's rule' in the mallard (*Anas platyrhynchos*). *CR Biol* **325**, 221–230.

De Margerie E, Robin JP, Verrier D, et al. (2004) Assessing a relationship between bone microstructure and growth rate: a fluorescent labelling study in the king penguin chick (*Aptenodytes patagonicus*). *J Exp Biol* **207**, 869–879.

De Ricqlès AJ (1976) On bone histology of fossil and living reptiles, with comments on its functional and evolutionary significance. In: *Morphology and Biology of Reptiles*. (eds Bellairs AA, Cox CB), pp. 123–150, London: Academic Press.

De Ricqlés A, et al. (1991) Comparative microstructure of bone. *Bone* **3**, 1–78.

Enlow D (1962) A study of the postnatal growth and remodeling of bone. *Am J Anat* **110**, 79–101.

Epker BN, Frost HM (1965) A histological study of remodeling at the periosteal, haversian canal, cortical endosteal, and trabecular endosteal surfaces in human rib. *Anat Rec* **152**, 129–135.

Frost H (1973) *Bone Modeling and Skeletal Modeling Errors. Orthopaedic Lectures*, Vol. **IV**. Springfield: Charles C Thomas.

Frost H (2001) From Wolff's Law to the Utah Paradigm: insights about bone physiology and its clinical applications. *Anat Rec* **262**, 398–419.

Garn S (1970) *The Earlier Gain and Later Loss of Cortical Bone*. Springfield: Thomas.

Garn S (1972) The course of bone gain and the phases of bone loss. *Orthop Clin North Am* **3**, 503–509.

Gocha TP, Agnew AM (2014) Evidence for regional asymptotes of osteon population density from the femoral midshaft. *Am J Phys Anthropol* **153**, 126.

Goldman HM, Bromage TG, Thomas CDL, et al. (2003a) Preferred collagen fiber orientation in the human mid-shaft femur. *Anat Rec* **272A**, 434–445.

Goldman HM, Bromage TG, Boyde A, et al. (2003b) Intrapopulation variability in mineralization density at the human femoral mid-shaft. *J Anat* **203**, 243–255.

Goldman HM, Thomas CD, Clement JG, et al. (2005) Relationships among microstructural properties of bone at the human midshaft femur. *J Anat* **206**, 127–139.

Goldman HM, McFarlin SC, Cooper DMI, et al. (2009) Ontogenetic patterning of cortical bone microstructure and geometry at the human mid-shaft femur. *Anat Rec* **292**, 24–64.

Goldman HM, Hampson NA, Guth JJ, et al. (2014) Intracortical remodeling parameters are associated with measures of bone robustness. *Anat Rec* **297**, 1817–1828.

Green SB, Salkind NJ (2008) *Using SPSS for Window and Macintosh: Analyzing and Understanding Data*, 5th edn. Upper Saddle River, NJ: Pearson Prentice Hall.

Gross TS, Srinivasan S, Liu CC, et al. (2002) Non-invasive loading of the murine tibia: an in vivo model for the study of mechanotransduction. *J Bone Miner Res* **17**, 493–501.

Herrmann B, Danielmeyer A (1994) Bone structures reflecting rhythm, seasonality, and life-style of past human populations. *Naturwissenschaften* **81**, 399–401.

Hohmann EL, Elde RP, Rysavy JA, et al. (1986) Innervation of periosteum and bone by sympathetic vasoactive intestinal peptide-containing nerve fibers. *Science* **232**, 868–870.

Iwaniec UT, Crenshaw TD, Schoeninger MJ, et al. (1998) Methods for improving the efficiency of estimating total osteon density in the human anterior mid-diaphyseal femur. *Am J Phys Anthropol* **107**, 13–24.

Jee WS, Tian XY, Setterberg RB (2007) Cancellous bone mini-modeling-based formation: a Frost, Takahashi legacy. *J Musculoskelet Neuronal Interact* **7**, 232–239.

Jones DB, Nolte H, Scholubbers JG, et al. (1991) Biochemical signal transduction of mechanical stain in osteoblast-like cells. *Biomaterials* **12**, 101–110.

Jowsey J (1966) Quantitative microradiography: a new approach in the evaluation of metabolic bone disease. *Am J Med* **40**, 485–491.

Lazenby RA (1990) Continuing periosteal apposition. I. Documentation, hypotheses, and interpretation. *Am J Phys Anthropol* **82**, 478–484.

Lee KC, Maxwell A, Lanyon LE (2002) Validation of a technique for studying functional adaptation of the mouse ulna in response to mechanical loading. *Bone* **31**, 407–412.

Maggiano CM (2012a) *Histomorphometry of Humeral Primary Bone: Evaluating the Endosteal Lamellar Pocket as an Indicator of Modeling Drift in Archaeological and Modern Skeletal Samples*. Columbus: The Ohio State University. PhD Thesis.

Maggiano CM (2012b) Making the mold: a microstructural perspective on bone modeling during growth and mechanical

adaptation. In: *Hard Tissue Histology: An Anthropological Perspective*. (eds Stout S, Crowder C), pp. 45–90, Boca Raton: CRC Press.

Maggiano CM, Maggiano IS, Kierdorf H, et al. (2008a). Identification of a distinct histomorphological feature of long bones: Potential applications in paleopathology and bioarchaeology. *Am J Phys Anthropol* **135** (Suppl), 145.

Maggiano IS, Schultz M, Kierdorf H, et al. (2008b) Cross-sectional analysis of long bones, occupational activities and long-distance trade of the Classic Maya from Xcambó – Archaeological and osteological evidence. *Am J Phys Anthropol* **136**, 470–477.

Maggiano CM, Maggiano IS, Stout S (2009) Quantitative histomorphometric evaluation of the endosteal lamellar pocket: comparing digital and point-count methods for the measurement of modeling drift remnants in the long bones of adult. *Am J Phys Anthropol* **44**(Suppl), 181.

Maggiano IS, Maggiano CM, Tiesler V, et al. (2011) A distinct region of microarchitectural variation in femoral compact bone: histomorphology of the endosteal lamellar pocket. *Int J Osteoarch* **21**, 743–750.

Maggiano CM, White CD, Longstaffe FJ (2013) High spatial resolution isotopic analysis of human primary bone: new methods for reconstructing short-term environmental and dietary change using the endosteal lamellar pocket. *Am J Phys Anthropol* **56**(Suppl), 186.

Martin RB, Burr DB, Sharkey NA (1998) *Skeletal Tissue Mechanics*. New York: Springer.

McFarlin SC, Terranova CJ, Zihlman AL, et al. (2008) Regional variability in secondary remodeling within long bone cortices of catarrhine primates: the influence of bone growth history. *J Anat* **213**, 308–324.

Meade JB, Cowin SC, Klawitter JJ, et al. (1984) Bone remodeling due to continuously applied loads. *Calcif Tissue Int* **36**(Suppl 1), S25–S30.

Merz W, Schenk R (1970) Quantitative structural analysis of human cancellous bone. *Acta Anat* **75**, 54–66.

Moore KL, Agur AMR, Dalley AF (2011) *Essential Clinical Anatomy*, 4th edn. New York: Lippincott Williams and Wilkins.

Newell-Morris L, Sirianni JE (1982) Parameters of bone growth in the fetal and infant macaque (*Macaca nemestrina*) humerus as documented by trichromatic bone labels. *Prog Clin Biol Res* **101**, 243–258.

Paine RR, Godfrey LR (1997) The scaling of skeletal microanatomy in non-human primates. *J Zool London* **241**, 803–821.

Parfitt AM (1983) The physiologic and clinical significance of bone histomorphometric data. In: *Bone Histomorphometry: Techniques and Interpretation*. (ed. Recker RR), pp. 143–244, Boca Raton: CRC Press.

Peck J, Stout S (2008) The effects of total hip arthroplasty on the structural and biomechanical properties of adult bone. *Am J Phys Anthropol* **138**, 221–230.

Pfeiffer S, Lazenby R, Chiang J (1995) Cortical remodeling data affected by sampling location. *Am J Phys Anthropol* **96**, 89–92.

Raguin E, Streeter M, Lazenby R, et al. (2014) Histomorphology of endosteal lamellar pocket: comparison of the second metacarpal in two genetically distinct populations. *Am J Phys Anthropol* **S58**, 124.

Robling A, Stout S (2003) Histomorphology, geometry, and mechanical loading in past populations. In: *Bone Loss and Osteoporosis: An Anthropological Perspective*. (eds Agarwal S, Stout S), pp. 189–205, New York: Kluwer Academic/Plenum Publishers.

Ruff C. B (no date) MomentMacroJ program [internet]. Available at: http://www.hopkinsmedicine.org/fae/mmacro.htm.

Ruff C, Holt B, Trinkaus E (2006) Who's afraid of the big bad Wolff?: 'Wolff's law' and bone functional adaptation. *Am J Phys Anthropol* **129**, 484–498.

Schultz M (1988) Methoden der Licht- und Elektronenmikroskopie. In: *Handbuch der vergleichenden Biologie des Menschen 1, 1*. (ed. Knussmann R), pp. 698–730, Stuttgart: G. Fischer.

Schultz M, Drommer R (1983) Möglichkeiten der Präparateherstellung aus dem Gesichtsschädelbereich für die makroskopische und mikroskopische Untersuchung unter Verwendung neuer Kunststofftechniken. In: *Fortschritte der Kiefer- und Gesichts-Chirurgie 28. Experimentelle Mund-Kiefer-Gesichts-Chirurgie. Mikrochirurgische Eingriffe*. (ed. Hoppe WG), pp. 95–97, Stuttgart: G. Thieme.

Skedros JG, Hunt KJ (2004) Does the degree of laminarity correlate with site-specific differences in collagen fibre orientation in primary bone? An evaluation in the turkey ulna diaphysis. *J Anat* **205**, 121–134.

Skedros JG, Mason MW, Bloebaum RD (2001) Modeling and remodeling in a developing artiodactyl calcaneus: a model for evaluating Frost's Mechanostat hypothesis and its corollaries. *Anat Rec* **263**, 167–185.

Srinivasan S, Weimer DA, Agans SC, et al. (2002) Low magnitude mechanical loading becomes osteogenic when rest is inserted between each load cycle. *J Bone Miner Res* **17**, 1613–1620.

Zar JH (2010) *Biostatistical Analysis*, 5th edn. New York: Pearson.